Heteroatom Chemistry
Volume 20, Number 6, 2009

New Tin(IV) Complexes with Sterically Hindered *o*-Iminobenzoquinone Ligand: Synthesis and Structure

Alexandr V. Piskunov,[1] Irina N. Mescheryakova,[1] Georgii K. Fukin,[1] Artyem S. Bogomyakov,[2] Galina V. Romanenko,[2] Vladimir K. Cherkasov,[1] and Gleb A. Abakumov[1]

[1]*G. A. Razuvaev Institute of Organometallic Chemistry of Russian Academy of Sciences, Tropinina str. 49, 603950, Nizhny Novgorod, GSP-445, Russia*

[2]*International Tomography Centre of SB Russian Academy of Sciences, Institutskaya str. 3a, 630090, Novosibirsk, Russia*

Received 14 May 2009; revised 25 August 2009

ABSTRACT: *The reduction of 4,6-di-tert-butyl-N-(2, 6-di-iso-propylphenyl)-o-iminobenzoquinone (imQ) by tin amalgam in hexane solution leads to new six-coordinated o-iminoquinonato tin(IV) complex* $(iSQ)_2SnAP$ (**1**) *(where iSQ and AP are o-iminosemiquinolate and dianion o-amidophenolate, respectively). Variable temperature magnetic susceptibility measurements of* **1** *have shown that this complex possesses a weak ferromagnetic exchange between o-iminosemiquinonate ligands. The oxidation of* **1** *with air oxygen produces new o-iminoquinonolate tin(IV) derivatives* $[(iSQ)Sn(AP)]_2O$ (**2**) *and* $(iSQ)_2Sn(OH)_2$ (**3**) *containing* μ*-oxo- and hydroxo-ligands, respectively. The electronic structure of* **1** *was examined by DFT analysis. Complexes* **1–3** *have been investigated using single-crystal X-ray diffraction.* © 2009 Wiley Periodicals, Inc. Heteroatom Chem 20:332–340, 2009; Published online in Wiley InterScience (www.interscience.wiley.com). DOI 10.1002/hc.20555

Correspondence to: Alexandr Piskunov; e-mail: pial@iomc.ras.ru.

Contract grant sponsor: Russian Foundation for Basic Research.
Contract grant numbers: 07-03-00711-a, 07-03-00819-a, and 06-03-32728-a.
Contract grant sponsor: Russian President Grant.
Contract grant number: NSh-4182.2008.3.
Contract grant sponsor: Civilian Research and Development Foundation.
Contract grant number: RUE1-2839-NO-06.

INTRODUCTION

This work was outcome of our interest in redox-active ligands particularly based on *o*-iminoquinones. During past years, the interest in the coordination chemistry of *o*-iminoquinones and their derivatives has increased a lot. The extensive data on *o*-iminoquinone complexes have been accumulated to date [1]. This type of ligands can coordinate to a metal ion in unreduced [2], one-electron reduced *o*-iminobenzosemiquinone radical (iSQ), and two-electron reduced *o*-amidophenolate (AP) forms. The use of *o*-iminosemiquinone as a spin label in metal complexes allows us to monitor complex composition, structure, and dynamic processes in coordination sphere by simple means of EPR spectroscopy [3]. On the other hand, *o*-iminosemiquinones can be considered as the magnetic centers. From this point of view, the investigation and analysis of magnetic exchange interactions between ligands are important. The application of main-group metals in such complexes allows obtaining pure ligand–ligand magnetic interactions, which are not complicated

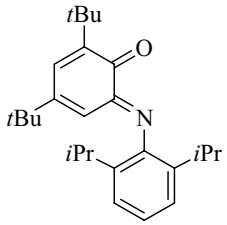

SCHEME 1

by paramagnetic metal ions. In recent communications, it was reported that disparate properties with respect to exchange coupling between *o*-iminobenzosemiquinone radicals coordinated to diamagnetic metal centers depend on the nature of metasubstituents at the innocent aniline moieties [4]. In addition, the introduction of the redox-active ligand into the main-group metal complex induces new reactivity of nontransition metal derivatives [4b, 5].

In accordance with aforesaid, the main-group metal chemistry of complexes based on 4,6-di-*tert*-butyl-*N*-(2,6-di-*iso*-propylphenyl)-*o*-iminoquinone ligand (imQ) (Scheme 1) is of interest.

Recently, the synthesis of germanium [6], tin [5c, 7], and antimony [5a,b] complexes on the basis of imQ containing one or two *o*-iminoquinone ligands was reported. In this paper, we present a tin derivative containing three imQ moieties and its oxidation by molecular oxygen.

RESULTS AND DISCUSSION

The nature of the solvent is known to be a crucial for products obtained in a reaction of 3,6-di-*tert*-butyl-*o*-benzoquinone with tin [8]. The interaction of *o*-iminoquinone (imQ) with tin amalgam in THF solution resulted in the formation of tin(IV) *o*-amidophenolate derivative (Scheme 2) [7a]. The analogous reaction being carried out in nonpolar hydrocarbons medium produces paramagnetic metal complex (**1**) (Scheme 2).

The reaction between tin amalgam and imQ in hexane is accompanied by color exchange from wine red to deep green. The 10-fold excess of metal amalgam allows completing this process during 1 h at room temperature. The complex **1** was obtained as green crystalline product from the hot hexane solution with a yield of approximately 40%. In contrast to transition metal derivatives that were unable to form tris-ligand derivatives of 4,6-di-*tert*-butyl-*N*−(2,6-dialkylphenyl)-*o*-iminobenzoquinones [1, 9], the tin complex **1** contains three ligands in different re-

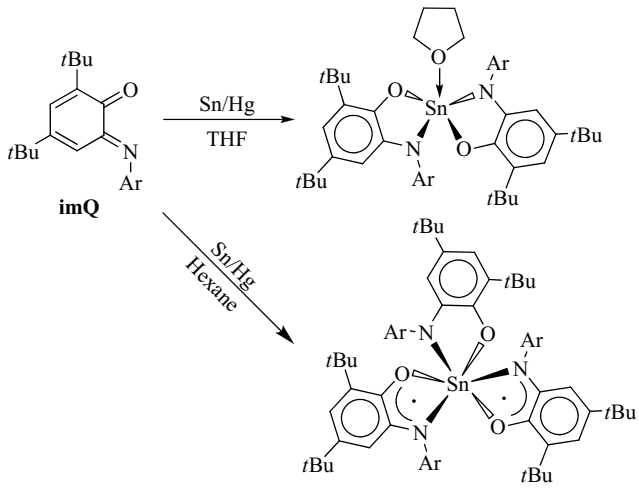

SCHEME 2

dox states. Two of them are radical-anion *o*-iminosemiquinolates and the last one is a dianionic *o*-amidophenolate. This is confirmed by the EPR spectra of this derivative. The anisotropic spectrum in frozen toluene matrix is typical for diradical derivatives (Fig. 1a). At 150 K, it exhibits half-field signal ($\Delta m_s = 2$) characteristic of diradicals. The zero-field splitting parameters of the $g = 2$ EPR signal (toluene, $D = 228$ G, $E = 43$ G, Fig. 1) allow to estimate the unpaired electron separation at

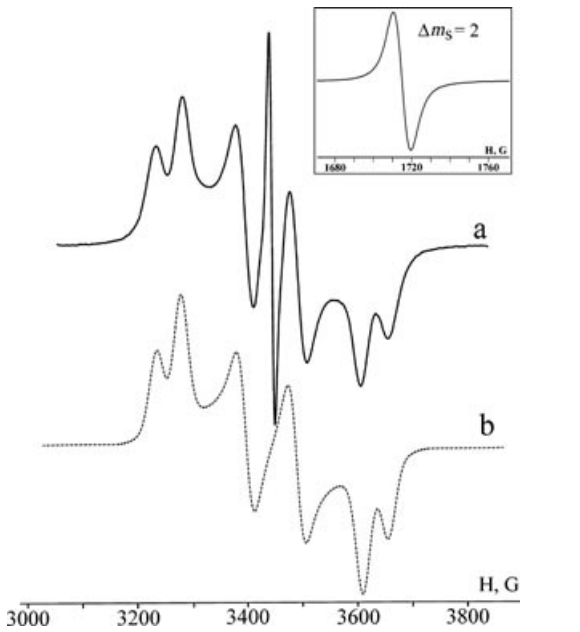

FIGURE 1 Experimental X-band EPR spectrum of **1** in toluene matrix at 150 K (a) and its simulation (b). Inset: $\Delta m_S = 2$ transition.

4.95 Å. In Near IR spectrum, the low-energy band is at 2060 nm. Such transitions are usual for mixed-valence metal complexes containing *o*-quinoid ligands in different redox states [1, 10].

The role of the solvent was clarified by our steric calculations [6] of $(AP)_2Sn$ (hypothetical complex), $(AP)_2Sn(THF)$ [7a], and complex **1**. The shielding of central metal (G-parameter) is 79.9(2)% and 93.7(2)% for $(AP)_2Sn$ (without THF molecule) and $(AP)_2Sn(THF)$ complexes, respectively. Consequently, there is enough space around the tin atom in the $(AP)_2Sn$ complex to accommodate of one THF molecule. At the same time, hexane (noncoordinated solvent) allows to associate the additional *o*-iminoquinone ligand with the formation of **1**. The G-parameter for **1** is 95.1(2)% and is noticeably more than for $(AP)_2Sn(THF)$. Thus, the competition for free coordination place between solvent molecules and ligands is observed. Hexane solvent leads to the formation of extremely sterically saturated complex **1** rather than $(AP)_2Sn$. Consequently, the $(AP)_2Sn$ complex is a sterically unsaturated, demanding subsequent stabilization of solvent molecules or ligands.

The molecular structure of **1** was determined by X-ray analysis. The selected bond lengths and angles are presented in Table 1. The crystal data collection and structure refinement data are listed in Table 2. All molecules in crystallographic unit cell of **1** are *fac*-isomers, and the tin atom has distorted prismatic environment (Fig. 2). The unit cell of **1** contains one disordered hexane molecule.

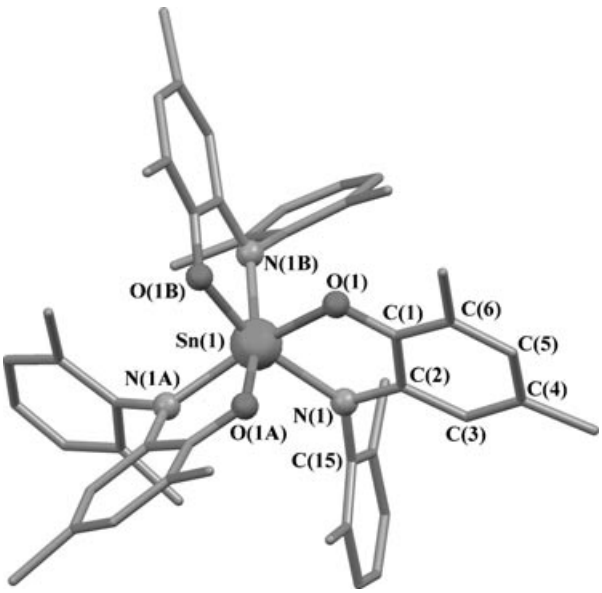

FIGURE 2 Molecular structure of complex **1**. H atoms and methyl groups of *i*-propyl and *t*-butyl substituents are omitted for clarity.

TABLE 1 Selected bond lengths (Å) and angles (°) of complexes **1–3**.

	1	**2**	**3**
		Bond	
Sn(1)–O(1)	2.072(3)	2.087(2)	2.1336(16)
Sn(1)–O(2)		2.008(2)	2.1253(17)
Sn(1)–O(3)		1.9265(4)	1.9827(18)
Sn(1)–O(4)			1.9728(17)
Sn(1)–N(1)	2.195(4)	2.143(2)	2.158(2)
Sn(1)–N(2)		2.065(2)	2.159(2)
N(1)–C(2)	1.383(7)	1.362(4)	1.336(3)
N(1)–C(15)	1.430(7)	1.489(4)	1.433(3)
N(2)–C(28)		1.355(4)	1.339(3)
N(2)–C(41)		1.415(3)	1.440(3)
O(1)–C(1)	1.321(5)	1.350(3)	1.303(3)
O(2)–C(27)		1.422(4)	1.296(3)
C(1)–C(2)	1.435(6)	1.445(5)	1.450(3)
C(1)–C(6)	1.394(7)	1.416(4)	1.426(3)
C(2)–C(3)	1.418(7)	1.309(5)	1.418(3)
C(3)–C(4)	1.357(9)	1.314(5)	1.359(3)
C(4)–C(5)	1.421(9)	1.526(5)	1.428(4)
C(5)–C(6)	1.382(8)	1.227(4)	1.371(4)
C(27)–C(28)		1.390(4)	1.456(4)
C(27)–C(32)		1.452(4)	1.431(4)
C(28)–C(29)		1.454(5)	1.416(3)
C(29)–C(30)		1.226(5)	1.362(4)
C(30)–C(31)		1.496(4)	1.432(4)
C(31)–C(32)		1.312(5)	1.378(3)
		Angle	
O(1)–Sn(1)–N(1)	77.95(16)	78.18(9)	75.52(7)
O(1)–Sn(1)–N(2)		89.29(9)	91.36(7)
O(2)–Sn(1)–N(1)		89.93(10)	88.80(7)
O(2)–Sn(1)–N(2)		80.36(9)	75.74(7)
O(2)–Sn(1)–O(1)		155.12(8)	81.82(6)
O(3)–Sn(1)–N(1)		112.56(11)	98.84(8)
O(3)–Sn(1)–N(2)		120.57(11)	95.06(8)
O(3)–Sn(1)–O(1)		99.93(6)	91.94(7)
O(3)–Sn(1)–O(2)		104.82(5)	168.67(7)
O(4)–Sn(1)–N(1)			93.49(7)
O(4)–Sn(1)–N(2)			97.24(7)
O(4)–Sn(1)–O(1)			166.40(7)
O(4)–Sn(1)–O(2)			90.09(7)
O(4)–Sn(1)–O(3)			97.74(8)
N(1)–Sn(1)–N(2)		126.75(8)	161.12(8)
C(1)–O(1)–Sn(1)	116.7(3)	114.05(19)	114.77(15)
C(27)–O(2)–Sn(1)		114.53(19)	116.26(16)
C(2)–N(1)–C(15)	114.3(4)	121.3(2)	119.5(2)
C(2)–N(1)–Sn(1)	109.5(3)	113.9(2)	114.67(16)
C(15)–N(1)–Sn(1)	134.2(4)	123.32(18)	125.70(15)
C(28)–N(2)–C(41)		119.9(2)	120.2(2)
C(28)–N(2)–Sn(1)		111.04(17)	114.94(16)
C(41)–N(2)–Sn(1)		129.0(2)	124.37(15)
Sn(1)–O(3)–Sn(1A)		177.47(18)	
O(1)–Sn–O(1A)	82.11(12)		
O(1)–Sn–N(1A)	159.99(11)		
O(1)–Sn–N(1B)	93.57(13)		
N(1)–Sn–N(1A)	104.67(13)		

The bases of antiprism are formed by parallel N(1)–N(1A)–N(1B) and O(1)–O(1A)–O(1B) planes. The distance between bases is 2.241 Å. The tin atom is shifted toward the plane of nitrogen atoms. The

TABLE 2 Summary of Crystal and Refinement Data for Complexes

Complex	*1 · Hexane*	*2 · Pentane*	**3**
Empirical formula	$C_{84}H_{125}N_3O_3Sn$	$C_{109}H_{160}N_4O_5Sn_2$	$C_{52}H_{76}N_2O_4Sn$
Formula weight	1415.62	1917.95	911.84
Temperature [K]	293(2)	218(1)	100(2)
Wavelength [Å]	0.71073	0.71073	0.71073
Crystal system	Rhombohedral	Monoclinic	Monoclinic
Space group	*R3*	*C2*	*P2(1)/c*
Unit cell dimensions			
a(Å)	16.016(3)	28.561(4)	20.1000(7)
b(Å)	16.016(3)	13.958(2)	11.9198(4)
c(Å)	27.400(5)	30.726(5)	22.1688(8)
α (°)	90	90	90
β (°)	90	117.281(2)	109.8830(10)
γ (°)	120	90	90
Volume (Å^3)	6086.7(19)	10887(3)	4994.8(3)
Z	3	4	4
Density (calculated) (g cm^{-3})	1.159	1.170	1.213
Absorption coefficient (mm^{-1})	0.364	0.510	0.555
Crystal size (mm^3)	0.20 × 0.20 × 0.10	0.80 × 0.20 × 0.20	0.12 × 0.10 × 0.08
Θ range for data collection (°)	1.65–23.31	0.75–26.45	1.88–26.00
Reflections collected	15,525	52,994	42,257
Independent reflections	3896 [R(int) = 0.0285]	22157 [R(int) = 0.0402]	9809 [R(int) = 0.0634]
Completeness (to Θ)	99.8% (23.31)	99.5% (26.45)	100.0% (26.00)
Absorption correction	None	None	Semi-empirical from equivalents
Maximum and minimum transmission			0.9570 and 0.9364
Refinement method	Full-matrix least-squares on F^2	Full-matrix-block least-squares on F^2	Full-matrix least-squares on F^2
Data/restraints/parameters	3896/1/275	22157/8/1127	9809/6/532
Final R indices [$I > 2\sigma(I)$] [a,b]	$R1 = 0.0378$, $wR2 = 0.0986$	$R1 = 0.0550$, $wR2 = 0.1077$	$R1 = 0.0460$, $wR2 = 0.0991$
R indices (all data)	$R1 = 0.0423$, $wR2 = 0.1045$	$R1 = 0.0636$, $wR2 = 0.1118$	$R1 = 0.0658$, $wR2 = 0.1050$
Goodness-of-fit on F^2 [c]	1.046	1.207	1.045
Largest diffraction peak and hole (e/Å^3)	0.352 and −0.437	1.054 and −1.099	0.794 and −0.554

[a] $R = \sum ||F_o| - |F_c|| / \sum |F_o|$. [b] $\omega R = R(\omega F^2) = \{\sum[\omega(F_o^2 - F_c^2)^2] / \sum [\omega(F_o^2)^2]\}^{1/2}$; $\omega = 1/[\sigma^2(F_o^2) + (aP)^2 + bP]$, $P = [2F_c^2 + \max(F_o, 0)]/3$.
[c] S = Goof = $\{\sum [\omega(F_o^2 - F_c^2)^2]/(n-p)\}^{1/2}$, where n is the number of reflections and p is the number of refined parameters.

distances between Sn(1) and N(1)–N(1A)–N(1B) and O(1)–O(1A)–O(1B) planes are 0.892 and 1.349 Å, respectively. It is necessary to note that this structure is the first example of prismatic composition among the metal tris-*o*-iminoquinonato complexes [1]. But the similar structure was observed for recently reported gallium(III) derivative with new hexadentate mono-*o*-iminosemiquinolate ligand [4b].

The molecule of **1** has a C_3 axis passing through Sn(1) atom. All three ligands are equal as the result. The dihedral angles between *o*-iminoquinoid ligands are 79.24°. The C(1)–O(1) (1.321(5) Å) and C(2)–N(1) (1.383(7) Å) distances are slightly longer than the corresponding bond lengths in known tin *o*-iminobenzosemiquinolates (1.292–1.303 and 1.334–1.342 Å [5c, 7b]) and are shorter than in *o*-amidophenolate tin complexes (C—O 1.361–1.399 Å, C—N 1.398–1.404 Å [7]). It should be noted that six-membered carbon rings C(1)C(6) are quite distorted. The quinoid pattern is observed: two shorter bonds are separated by longer bonds (see Table 1). The Sn(1)–O(1) (2.075(3) Å) distance is also intermediate between tin-to-*o*-amidophenolate [7] and tin-to-*o*-iminobenzosemiquinolate [5c, 7b] type bonding. Sn(1)–N(1) (2.195(4) Å) is significantly longer than for known *o*-iminoquinonato tin derivatives [5c, 7]. It is caused by the increase in steric repulsion between *cis*-located 2,6-di-*iso*-propyphenyl ligands ($G = 95.1(2)\%$).

So, structural features of ligands reveal mixed-valent state with different oxidation levels of ligands: two are radical-anions *o*-iminobenzosemiquinolates and the third one is dianion *o*-amidophenolate. At the same time, the structural equivalence of

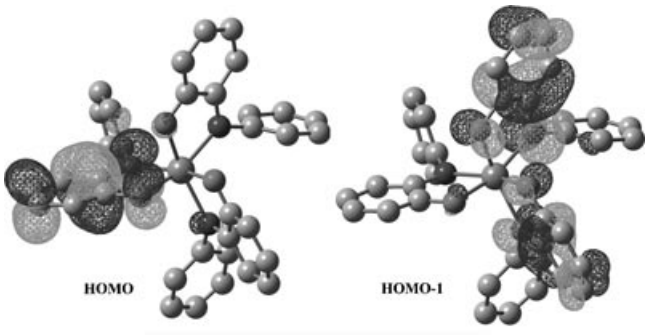

FIGURE 3 Representation of the frontier orbitals, HOMO and HOMO-1 of **1** from DFT calculations.

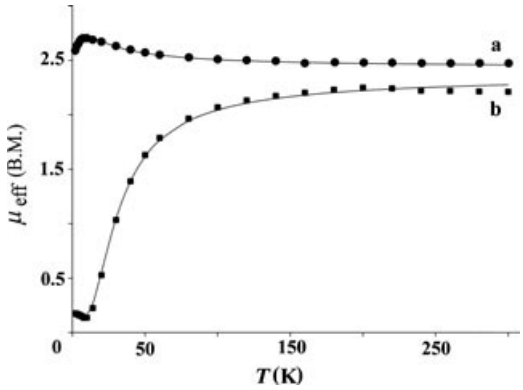

FIGURE 4 Dependences $\mu_{eff}(T)$ for **1** (a) and $(iSQ)_2SnPh_2$ (b). Solid lines demonstrate theoretical curves.

ligands reflects a charge delocalization over the whole molecule. The similar situation was observed recently for a germanium complex (iSQ)Ge(AP)Cl [6]. The electronic structure of complex **1** was examined by DFT calculations. Calculations were performed at the B3LYP/DGDZVP level using a C_3 molecule for complex **1** with unsubstituted phenyl groups as a model system for both singlet and triplet ground states of the molecule. The triplet ground-state configuration appears to be 9.4 kcal/mol more stable than the lowest singlet state. The calculated ground state for complex **1** agrees well with the magnetic susceptibility measurements data (see later). Two semioccupied MOs of the triplet system (HOMO (−0.194 eV) and HOMO-1 (−0.196 eV)) are shown on the Fig. 3. The HOMO orbital is localized on the one imQ ligand, whereas the HOMO-1 is delocalized between another two ligands. This delocalization promotes the orthogonalization of magnetic orbitals and leads to the triplet ground state for **1**. Thus the dihedral angle between plane of one *o*-iminoquinoid ligand and plane based on another two ligands is 89.45°. Our calculations are confirmed by the EPR data. The radical separation estimated from the anisotropic EPR spectra (4.95 Å) does not comply with "centroid(C(1)–C(6), N(1), O(1)) to centroid (C(1A)–C(6A), N(1A), O(1A))" distance between two *o*-iminoquinonato ligands in complex **1** obtained from X-ray structure (5.84 Å). However, it is in rather good agreement with centroid-to-centroid distance (5.06 Å) when the second centroid (C(1A)–C(6A), N(1A), O(1A), C(1B)–C(6B), N(1B), O(1B)) was calculated on the basis of another two ligands.

Temperature dependences of the effective magnetic moment (μ_{eff}) for complexes **1** and another hexacoordinated bis-*o*-iminosemiquinolate complex $(iSQ)_2SnPh_2$ [5c] are presented in Fig. 4 (magnetic data for the $(iSQ)_2SnPh_2$ complex is presented for comparison).

The increased μ_{eff} at lower temperatures points to the ferromagnetic exchange interactions (J = 7.9 cm^{-1}) between unpaired electrons of radicals in **1**. The magnetic studies reveal a weak ferromagnetic interaction between radical centers as contrasted with the computed triplet–singlet gap. The more enhanced calculation methods are necessary to solve this conflict. It will be the object of the subsequent investigations. For $(iSQ)_2SnPh_2$, μ_{eff} decreases at reduced temperatures due to antiferromagnetic exchange interactions (J = −29.9 cm^{-1}). Differences in character of exchange interactions are caused by structural changes in examined complexes. The distorted octahedral environment in $(iSQ)_2SnPh_2$ leads to the decrease in the dihedral angle between paramagnetic ligands (57.02° [5c]) in comparison with **1** (see earlier). This configuration promotes effective overlapping between magnetic orbitals and results in antiferromagnetic exchange in the $(iSQ)_2SnPh_2$ complex. Such conception is in good agreement with magnetic properties of another known octahedral tin bis-*o*-iminosemiquinolate derivative $(iSQ)_2SnCl_2$ [11]. The increase in the angle between radical ligands (66.79°) enhances a ferromagnetic contribution, and the simultaneous decrease in an antiferromagnetic contribution results in spin exchange (J = −3.8 cm^{-1}) [11]. It is necessary to note that the complex **1** is a one of the rare examples of the ferromagnetic interactions between radical anion ligands on the main-group metal [12]. Previously, the ferromagnetic behavior of tris-*o*-semiquinolate gallium [12a–c] and aluminum [12c] derivatives was reported. The ferromagnetic exchange was observed for tin(IV) and germanium(IV) complexes based on a radical ONO-ligand [12d].

Recently, we have reported the oxidation of tin(IV) *o*-amidophenolate complexes with oxygen

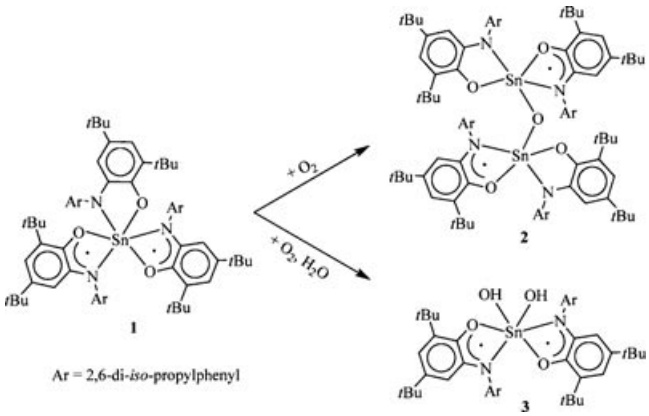

SCHEME 3

and sulfur that leads to the formation of new paramagnetic metal derivatives [5c]. The complex **1** can be oxidized by air oxygen to different products depending on reaction conditions (Scheme 3).

The reaction with dry oxygen gives binuclear μ-oxo-tin complex **2**, whereas the crystallization of **1** from diethyl ether solution by its slow evaporation on air conditions resulted in the formation of dihydroxo derivative **3**. The presence of OH groups in **3** was confirmed by sharp lines in IR spectrum at 3642 cm^{-1}.Compounds **2** and **3** have anisotropic spectra in frozen toluene matrix, typical for diradical derivatives (Fig. 5). At 150 K, they exhibit half-field signal ($\Delta m_s = 2$) characteristic of diradicals. The zero-field splitting parameters of the $g = 2$ EPR signal ($D = 61$ G, $E \approx 0$ G for **2** and $D = 165$ G, $E \approx 0$ G for **3**) allow to estimate the unpaired electron separation at 7.69 and 5.52 Å for **2** and **3**, respectively. These values are in good agreement with those obtained from the structural investigation of the data (7.59 and 5.44 Å).

Molecular structures of **2** and **3** are shown in Figs. 6–8. Selected bond lengths and angles are given in Table 1. The crystal data collection and structure refinement data are listed in Table 2. Crystals suitable for X-ray analysis were obtained from pentane (**2**) and diethyl ether (**3**).

There are two crystallographic unique molecules in the asymmetric unit of **2** (Fig. 6). The angels and bond lengths of both units are quite similar. The main difference between **A** and **B** molecules is the Sn–O–Sn angle, which is 159.9(2) and 177.47(18), respectively. In the sequel, the only **B** molecule is discussed. Also the unit cell of complex **2** contains pentane solvate molecules.

The molecule of complex **2** lies on the inversion center, and both tin atoms have identical distorted

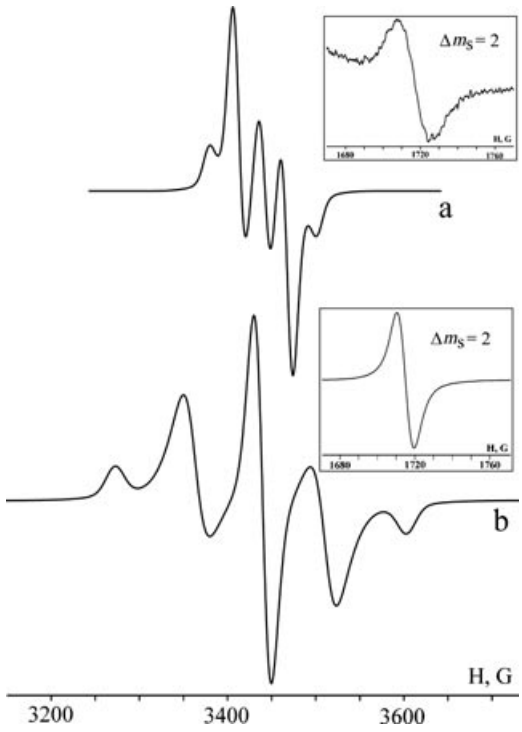

FIGURE 5 Experimental X-band EPR spectrum of **2** (a) and **3** (b) in toluene matrix at 150 K. Insets: $\Delta m_s = 2$ transitions.

trigonal bipyramidal environment (Figs. 6 and 7). The nitrogen atoms and the oxo-group form the pyramid base, while oxygen atoms of chelate ligands occupy apical sites. The heteroatom-to-tin-to-heteroatom angles reveal the difference as usual for five-coordinate transition metal complexes of the ML_2X type [1] (where L is *o*-iminobenzoquinonato-based ligand): angle N(1)–Sn(1)–N(2) of 126.75(8)° is less than O(1)–Sn(1)–O(2) of 155.12(8)°. The dihedral angle between *o*-iminoquinoid ligands is 43.69°, that is significantly less than for another five-coordinated (AP)Sn(iSQ)Ph complex (59.13°) [5c].

One of the *o*-iminoquinoid ligands in a half of **2** is dianion *o*-amidophenolate. The distances O(2)–C(27) of 1.422(4) Å and N(2)–C(28) of 1.355(4) Å

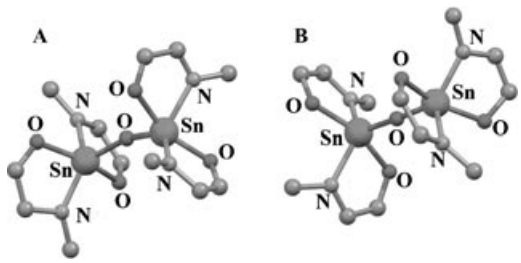

FIGURE 6 Fragments of structure of two independent units in crystal of **2**.

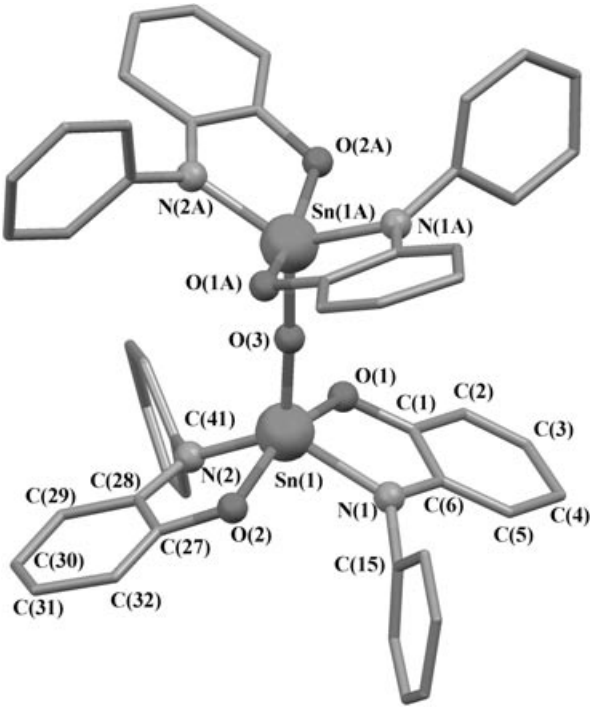

FIGURE 7 Molecular structure of complex **2**. H atoms, *i*-propyl and *t*-butyl substituents are omitted for clarity.

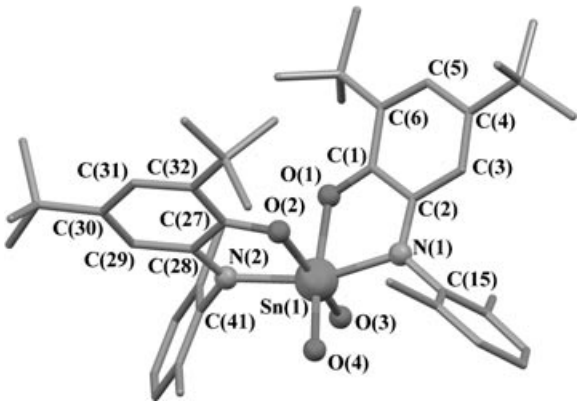

FIGURE 8 Molecular structure of complex **3**. Methyl groups of *i*-propyl substituents and H atoms are omitted for clarity.

are closer to those distances in *o*-amidophenolato tin(IV) complexes [7]. The second ligand shows the structural features of *o*-iminosemiquinonato ligand. While the N(1)–C(2) distance is approximately the same as in *o*-amidophenolate ligand (1.362(4) Å), the O(1)–C(1) (1.350(3) Å) bond is significantly shortened in comparison with O(2)–C(27) and is typical for *o*-iminosemiquinonato metal complexes [1]. The Sn(1)–O(2) and Sn(1)–N(2) covalent bonds (2.008(2) and 2.065(2) Å, respectively) are quite shorter than Sn(1)–O(1) and Sn(1)–N(1) (2.087(2) and 2.143(2) Å, respectively) which is indicative of different nature of *o*-iminoquinoid ligands. The longer Sn—N and Sn—O bonds are characteristic for radical-anion form of the ligand.

Two (AP)Sn^{IV}(iSQ) halves are bridged by a μ-oxo group (Sn(1)–O(3)–Sn(1A) is 177.47(18)°), which is close to those (175.2(2)°) obtained in related binuclear iron complex containing two *o*-iminosemiquinonato ligands per metal atom [13]. The Sn(1)–O(3) bond length (1.9265(4) Å) lies in the range 1.90–1.95 Å, typical for stannoxane derivatives [14]. The centroid-to-centroid distance between *o*-iminosemiquinoid ligands located in different parts of binuclear molecule is 7.58 Å.

A central tin atom in **3** (Fig. 8) has a distorted octahedral environment and is composed of two O,N-coordinated *o*-iminobenzosemiquinonato ligands and two hydroxyl groups. The dihedral angle between *o*-iminosemiquinoid ligands is 69.42°. The centroid-to-centroid distance between these radical-anions is 5.44 Å.

The Sn(1)–O(1, 2) and Sn(1)–N(1, 2) distances at 2.1336(16), 2.1253(17) Å and 2.158(2), 2.159(2) Å, respectively, are close to those obtained for known Sn(IV) *o*-iminosemiquinonate complexes [5c, 7b]. Bond lengths C—O and C—N of *o*-iminoquinone ligands in **3** (Table 1) are indicative of O,N-coordinated *o*-iminobenzosemiquinonato radical-anions (C—O 1.29–1.33 Å, C—N 1.33–1.35 Å) [1]. These bonds in **3** are significantly shorter than bonds expected for coordinated *o*-amidophenolates (C—O 1.35–1.36 Å, C—N 1.38–1.39 Å) or its N-protonated *o*-aminophenolate form (C—O 1.35–1.36 Å, C—N 1.42–1.47 Å) [1]. In addition, nitrogen atoms are three-coordinate and sp^2-hybridized, the sums of angles about nitrogens are 359.9(5)° and 359.5(5)°. In both ligands, the C—C distances in rings C(1)C(6) and C(27)C(32) are not equidistant and show a quinoid-type alternation (see Table 1).

It is noteworthy that hydroxyl groups are in *cis*-position to each other, and the angle O(3)–Sn(1)–O(4) is 97.74(8)°. At the same time, *o*-iminosemiquinonato ligands are situated in such a manner that nitrogen atoms are trans-located and the N(1)–Sn(1)–N(2) angle has a value of 161.12(8)° (Fig. 7). It is remarkable that the *cis*-position of nitrogen atoms could lead to the significant increase of sterical repulsion between 2,6-di-*iso*-propylphenyl fragments. It is interesting to note that the complex **3** does not contain additional coordinated H_2O molecules in spite of its presence during oxidation and crystallization process. Apparently, it can be caused by insufficient space around the Sn atom to

accommodate H_2O. Our calculations of solid angles have shown that G-parameter for **3** is 95.1(2)%. Consequently, nonbonding ligand–ligand interactions in a coordination sphere of Sn prevent this process.

CONCLUSION

In present paper, it has been shown that bulky aryl-substituted *o*-iminoquinone imQ can form the hexacoordinated tris-ligand complex with the tin(IV) ion. The weak ferromagnetic exchange between two radicals in this derivative has been observed. The oxidation of the complex described above by molecular oxygen leads to the binuclear μ-oxo-derivative or dihydroxy in the presence of air moisture.

EXPERIMENTAL

General

All reagents were of analytical grade. Solvents were purified by following the standard methods [15]. 4,6-Di-*tert*-butyl-*N*-(2,6-di-*iso*-propylphenyl)-*o*-iminobenzoquinone (imQ) [16] was prepared according to the known procedure. All manipulations on complexes were performed in vacuum under oxygen- and moisture-free conditions.

The infrared spectra of complexes in the 8000–400 cm^{-1} range were recorded on a FSM 1201 Fourier-IR spectrometer in mineral oil (Nujol). EPR spectra were recorded on a Bruker EMX spectrometer.

The magnetic susceptibility of the polycrystalline complexes was measured with a Quantum design MPMS*XL* SQUID magnetometer in the temperature range 2–300 K with magnetic field of up to 5 kOe. None of complexes exhibited any field dependence of molar magnetization at low temperatures. Diamagnetic corrections were made using the Pascal constants. The effective magnetic moment was calculated as $\mu_{eff}(T) = [(3k/N_A\mu_B^2)\chi T]^{1/2} \approx (8\chi T)^{1/2}$.

Complex **1**. The imQ (1.52 g, 4 mmol) dispersion in hexane (30 mL) was added to tin (4.75 g, 40 mmol) amalgam, and the reaction mixture was shaken for about 1 h. During the reaction, the color of solution turned from red to deep green. After completion of the reaction (the color of reaction mixture did not change any more), the solution was concentrated under reduced pressure and deep green crystals of **1** were obtained by filtration. Additional portions of **1** can be obtained by following the same procedure from the filtrate solution. The total yield of 1·hexane was 0.78 g (41.7%) of the analytically pure compound. Mp 136°C (dec.). Anal. calcd for $C_{84}H_{125}N_3O_3Sn$: C, 75.09; H, 9.38; N, 3.13; O, 3.57; Sn, 8.84. Found: C, 75.36; H, 9.45; Sn, 8.59. Near IR (Nujol, nm): ~2060 nm. IR (Nujol, cm^{-1}): 1585 s, 1564 m, 1436 s, 1419 m, 1360 s, 1337 m, 1289 m, 1251 s, 1239 m, 1203 w, 1173 m, 1109 m, 1056 w, 1020 w, 994 w, 973 s, 957 w, 933 w, 919 w, 859 m, 843 w, 798 s, 767 m, 676 w, 654 w, 613 w, 550 w, 503 w.

Complex **2**. The solution of complex **1** (0.5 g, 0.4 mmol) in pentane (30 mL) was exposed to dry oxygen (20 mL, 0.9 mmol). The reaction mixture was stirred for 1 h, and solution was deaerated. The deep green crystals of **2** were collected after storing of the solution at −18°C over night. The yield of 2·pentane was 0.22 g (56.4%). Mp 162°C (dec.). Anal. calcd for $C_{109}H_{160}N_4O_5Sn_2$: C, 71.00; H, 8.75; N, 3.04; O, 4.34; Sn, 12.88. Found: C, 71.16; H, 8.92; Sn, 12.65. Near IR (Nujol, nm): ~1900 nm. IR (Nujol, cm^{-1}): 1426 s, 1378 s, 1362 s, 1328 m, 1282 m, 1253 m, 1200 w, 1179 w, 1168 w, 1112 w, 1081 w, 1056 w, 1043 w, 1028 w, 992 w, 937 w, 914 w, 877 w, 864 w, 824 w, 799 s, 768 w, 742 w, 668 w, 650 w, 634 w, 609 w, 586 m, 548 w, 500 w.

Complex **3**. The solution of complex **1** (0.5 g, 0.4 mmol) in diethyl ether (20 mL) was slowly evaporated under air conditions. Complex **3** deposits were obtained from the solution as deep-green crystals. 0.23 g of compound **3** was obtained (yield 63.1%). Mp 178°C (dec.). Anal. calcd for $C_{52}H_{76}N_2O_4Sn$: C, 68.49; H, 8.40; Sn, 13.02. Found: C, 68.75; H, 8.42; Sn, 13.17. IR (Nujol, cm^{-1}): 3642 s, 1582 s, 1428 s, 1390 s, 1361 s, 1328 s, 1254 s, 1198 m, 1173 m, 1112 m, 1100 w, 1057 w, 1044 w, 1028 w, 994 w, 936 w, 913 m, 876 w, 864 m, 834 m, 820 m, 797 s, 767 m, 742 w, 722 w, 708 w, 672 w, 646 w, 634 w, 609 w, 584 s, 499 m.

DFT Calculations

DFT calculations reported here were performed with the Orca program package [17] using the B3LYP hybrid functional at DGDZVP level theory.

X-Ray Crystallographic Study of **1**−**3**

Intensity data for **1–3** were collected on a Smart Apex diffractometer with graphite monochromated Mo K_α radiation ($\lambda = 0.71073$ Å) in the φ-ω scan mode ($\omega = 0.3°$, 10 s on each frame). The intensity data were integrated by the SAINT program [18]. SADABS [19] was used to perform area-detector scaling and absorption corrections. The structures of **1–3** were determined by direct methods and were refined on F^2 using all reflections with the SHELXTL package [20]. All nonhydrogen atoms were refined

anisotropically. The hydrogen atoms in **1–3** were placed at calculated positions and were refined in the riding model. The hexane molecule in a crystal unit of complex **1** is disordered. The hydrogen atoms in the hexane molecule were not disclosed, and carbon atoms were refined isotropically. Selected bond distances and angles for **1–3** are given in Table 1. Table 2 summarizes the crystal data and some details of the data collection and refinement for these complexes.

SUPPLEMENTARY MATERIAL

CCDC 712211 (**1**), 712212 (**2**), 712213 (**3**) contain the supplementary crystallographic data for this paper. These data can be obtained free of charge at www.ccdc.cam.ac.uk/conts/retrieving.html [or from the Cambridge Crystallographic Data Center, 12, Union Road, Cambridge CB2 1EZ, UK; fax: (international) +44-1223/336-033; E-mail: deposit@ccdc.cam.ac.uk].

REFERENCES

[1] Poddel'sky, A. I.; Cherkasov, V. K.; Abakumov, G. A. Coord Chem Rev 2009, 253, 291–324.
[2] Mukherjee, C.; Weyhermüller, T.; Bothe, E.; Chaudhuri, P. Inorg Chem 2008, 47, 2740–2746.
[3] Poddel'sky, A. I.; Cherkasov, V. K.; Bubnov, M. P.; Abakumova, L. G.; Abakumov, G. A. J Organomet Chem 2005, 690, 145–150.
[4] (a) Chaudhuri, P.; Wagner, R.; Pieper, U.; Biswas, B.; Weyhermüller, T. Dalton Trans 2008, 1286–1288; (b) Chaudhuri, P.; Bill, E.; Wagner, R.; Pieper, U.; Biswas, B.; Weyhermüller, T. Inorg Chem 2008, 47, 5549–5551.
[5] (a) Abakumov, G. A.; Poddel'sky, A. I.; Grunova, E. V.; Cherkasov, V. K.; Fukin, G. K.; Kurskii, Y. A.; Abakumova, L. G. Angew Chem, Int Ed 2005, 44, 2767–2771; (b) Cherkasov, V. K.; Abakumov, G. A.; Grunova, E. V.; Poddel'sky, A. I.; Fukin, G. K.; Baranov, E. V.; Kurskii, Y. A.; Abakumova, L. G. Chem Eur J 2006, 12, 3916–3927; (c) Piskunov, A. V.; Mescheryakova, I. N.; Fukin, G. K.; Baranov, E. V.; Hummert, M.; Shavyrin, A. S.; Cherkasov, V. K.; Abakumov, G. A. Chem Eur J 2008, 14, 10085–10093.
[6] Piskunov, A. V.; Aivaz'yan, I. A.; Poddel'sky, A. I.; Fukin, G. K.; Baranov, E. V.; Cherkasov, V. K.; Abakumov, G. A. Eur J Inorg Chem 2008, 1435–1444.
[7] (a) Piskunov, A. V.; Aivaz'yan, I. A.; Fukin, G. K.; Baranov, E. V.; Shavyrin, A. S.; Abakumov, G. A.; Cherkasov, V. K. Inorg Chem Commun 2006, 9, 612–615; (b) Piskunov, A. V.; Aivaz'yan, I. A.; Abakumov, G. A.; Cherkasov, V. K.; Kuznetsova, O. V.; Fukin, G. K.; Baranov, E. V. Russ Chem Bull 2007, 56, 261–266.
[8] Piskunov, A. V.; Lado, A. V.; Fukin, G. K.; Baranov, E. V.; Abakumova, L. G.; Cherkasov, V. K.; Abakumov, G. A. Heteroatom Chem 2006, 17, 481–490.
[9] (a) Poddel'sky, A. I.; Cherkasov, V. K.; Fukin, G. K.; Bubnov, M. P.; Abakumova, L. G.; Abakumov, G. A. Inorg Chim Acta 2004, 357, 3632–3640; (b) Abakumov, G. A.; Poddel'sky, A. I.; Bubnov, M. P.; Fukin, G. K.; Abakumova, L. G.; Ikorskii, V. N.; Cherkasov, V. K. Inorg Chim Acta 2005, 358, 3829–3840.
[10] (a) Pierpont, C. G. Coord Chem Rev 2001, 219–221, 415–433; (b) Pierpont, C. G. Coord Chem Rev 2001, 216–217, 99–125; (c) Lange, C. W.; Conklin, B. J.; Pierpont, C. G. Inorg Chem 1994, 33, 1276–1283.
[11] Lado, A. V.; Poddel'sky, A. I.; Piskunov, A. V.; Fukin, G. K.; Baranov, E. V.; Ikorskii, V. N.; Cherkasov, V. K.; Abakumov, G. A. Inorg Chim Acta 2005, 358, 4443–4450.
[12] (a) Adams, D. M.; Rheingold, A. L.; Dei, A.; Hendrickson, D. N. Angew Chem, Int Ed 1993, 32, 391–392; (b) Ozarowski, A.; McGarvey, B. R.; El-Hadad, A.; Tian, Z.; Tuck, D. G.; Krovich, D. L.; DeFotis, G. C. Inorg Chem 1993, 32, 841–847; (c) Lange, C. W.; Conklin, B. J.; Pierpont, C. G. Inorg Chem 1994, 33, 1276–1283; (d) Bruni, S.; Caneschi, A.; Cariati, F.; Delfs, C.; Dei, A.; Gatteschi, D. J Am Chem Soc 1994, 116, 1388–1394.
[13] Mukherjee, S.; Weyhermüller, T.; Wieghardt, K.; Chaudhuri, P. Dalton Trans 2003, 3483–3485.
[14] (a) Glidewell, C.; Liles, D. C. Acta Crystallogr B 1978, 34, 1693–1695; (b) Glidewell, C.; Liles, D. C. Acta Crystallogr B 1979, 35, 1689–1691; (c) Lockhart, T. P.; Puff, H.; Schuh, W.; Reuter, H.; Mitchell, T. N. J Organomet Chem 1989, 366, 61–72.
[15] Perrin, D. D.; Armarego, W. L. F.; Perrin, D. R. Purification of Laboratory Chemicals; Pergamon: Oxford, UK, 1980.
[16] Abakumov, G. A.; Druzhkov, N. O.; Kurskii, Yu. A.; Shavyrin, A. S. Russ Chem Bull 2003, 52, 712–717.
[17] Neese, F. ORCA: An ab initio, density functional and semiempirical program package, v. 2.3, rev. 09; Max Planck Institut für Strahlenchemie, Mülheim, Germany, 2004.
[18] Bruker. SAINTPlus Data Reduction and Correction Program, v. 6.02a; Bruker AXS: Madison, WI, 2000.
[19] Sheldrick, G. M. SADABS, v.2.01, Bruker/Siemens Area Detector Absorption Correction Program; Bruker AXS: Madison, WI, 1998.
[20] Sheldrick, G. M. SHELXTL, v. 6.12, Structure Determination Software Suite; Bruker AXS: Madison, WI, 2000.